LANGMUIR

Article

pubs.acs.org/Langmuir

Lipid Vesicle Interaction with Hydrophobic Surfaces: A Coarse-Grained Molecular Dynamics Study

Ilaria Mannelli,*[,†] Francesc Sagués,[‡] Valerio Pruneri,[†,§] and Ramon Reigada*[,‡,∥]

[†]ICFO-Institut de Ciències Fotòniques, The Barcelona Institute of Science and Technology, Castelldefels Barcelona 08860, Spain

[‡]Departament de Ciència dels Materials i Química Física and [∥]Institut de Química Teòrica i Computacional (IQTCUB), Universitat de Barcelona, c/Marti i Franqués 1, Pta 4, 08028 Barcelona, Spain

[§]ICREA-Institució Catalana de Recerca i Estudis Avançats, Passeig Lluís Companys, 23, 08010 Barcelona, Spain

ABSTRACT: Active surfaces are presently tailored to cause specific effects on living cells, which can be useful in many fields. Their development requires the understanding of the molecular mechanisms of interaction between lipid-enveloped entities and solid surfaces. Here, using coarse-grained molecular dynamics simulations, we have analyzed the different interaction modes of coated substrates with lipid vesicles that mimic biological envelopes. For neutral and hydrophobically functionalized substrates, three action modes on contacting vesicles have been obtained including intact, partially broken, and completely destroyed vesicles. The molecular mechanisms for each interaction pathway and the corresponding energy balances have been analyzed in detail. Interestingly, we have shown that any specific action mode can be obtained by appropriately tailoring the wetting characteristics of the surface coating. In particular, we have shown that surfaces that are simultaneously hydrophobic and oleophilic are optimal to fully disrupt the contacting vesicle lipid bilayer.

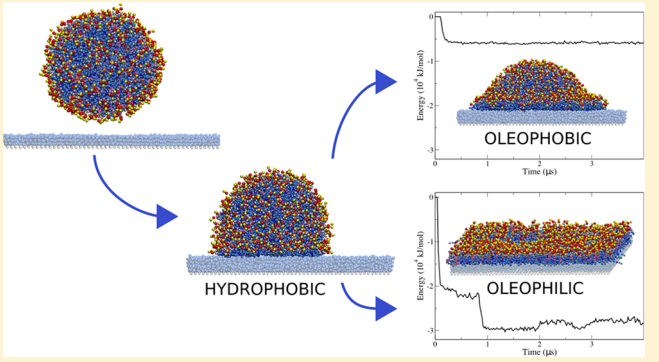

1. INTRODUCTION

The ability of living cells to interact with different surfaces is an important area of study in many scientific fields such as medicine,[1] materials engineering,[2] and environmental sciences.[3] Despite the importance of cell−solid substrate interactions, the fundamental molecular-scale mechanisms taking place at the interface are still poorly understood. Basic in vitro systems such as model lipid membranes mimicking biological surfaces have been used for this purpose. In this context, two different scenarios can be envisaged, depending on whether the contacting surface displays a favorable interaction with the membrane lipid headgroups. As an example of a favorable interaction, the deposition and adsorption of unilamellar model lipid vesicles from an aqueous solution to an attractive surface is one of the most common techniques to form supported lipid bilayers,[4] which is widely used as research platforms that enable in vitro investigation of membrane-related processes as well as biocompatible and biofunctional coatings on solid substrates.[5−7] However, an unfavorable interaction with hydrophobic surfaces is suggested to eventually result in membrane destruction to gain direct access to the inner hydrophobic part of the lipid bilayer assembly. This effect has been hypothesized to be responsible for several observations such as the antibacterial activity of graphene oxide sheets[8] and the inactivation effect of hydrophobic polycation coatings on pathogenic bacteria and influenza virus.[9,10] Moreover, in a recently published paper, we have reported that silica surfaces (SURFs) functionalized with neutral alkyl- and fluoro-silanes exhibit strong antiviral properties.[11] Interestingly, although the main hypothesis to explain microorganism inactivation is based on the hydrophobicity of the neutral solid substrate, the latter study revealed that highly hydrophobic fluorinated moieties are less effective than alkane-based coatings. Therefore, other surface characteristics in addition to hydrophobicity must be taken into account to understand the interaction between the microorganism lipid envelope and the contacting substrate.

Experimental difficulties in unveiling the ultimate molecular mechanisms regulating the behavior of interacting systems are generally overcome by the use of molecular-level computer simulations. For example, molecular dynamics (MD) simulations have become a powerful technique to provide direct insights into many lipid membrane processes at the molecular-level. Whereas atomistic MD simulations are limited to short time scales (a few hundreds of nanoseconds) and length scales (10−20 nm), coarse-grained (CG) MD cover much longer scales, still preserving the main molecular characteristics of the simulated moieties. CG models have been widely used in the study of the interactions of lipid bilayers with different solid supports, and they have served to elucidate the influence of surface roughness and topology on the supported bilayer

Received: September 12, 2016
Revised: October 24, 2016
Published: November 3, 2016

DOI: 10.1021/acs.langmuir.6b03364
Langmuir XXXX, XXX, XXX−XXX

behavior at the molecular-level.[12−16] In the context of lipid vesicles, the spatiotemporal scales achieved in CGMD simulations may allow capturing, for instance, eventual adhesion, deposition, or destruction processes resulting from their contact with solid substrates. To date, however, molecular simulations of lipid vesicles in contact with solid substrates are limited to three studies, two of them using dissipative particle dynamics by Wu et al.[17] and Fuhrmans and Müller,[18] and a recent MD study by Liu et al.[19] In these studies, attractive (hydrophilic and/or charged) surfaces were simulated, and the process of formation of supported lipid bilayers was analyzed. In addition, we elucidated[11] through CG MD simulations the effect of functionalized surfaces on viral particles and found a good agreement with experimental data. However, a systematic study made with molecular-level approaches for the interaction with nonattractive substrates is still lacking, and this is the motivation for the present work.

In this paper, a systematic collection of CG-MD simulations is presented to study the interaction between simple lipid vesicles and a variety of solid substrates. Both the molecular mechanisms of vesicle conformation changes and their associated energy balances are analyzed. The physicochemical characteristics of the contacting surfaces are tailored by coating them with self-assembled monolayers (SAMs) of a series of neutral molecules displaying different lengths and at different surface densities (number of molecules per surface area). Our purpose is to analyze the action of coated substrates on the contacting lipid vesicle in terms of their wetting properties. For this reason, simulations for the determination of contact angles (CAs) of water and oil [hexadecane (HD)] droplets on the coated surfaces are also performed. We address mostly the case of nonhydrophilic substrates and therefore the characterization of eventual bilayer disruption and further vesicle destruction upon contact. Our results from the study of the interaction pathways and the energy analysis as well as their correlation with the water and oil CAs show the importance of both surface hydrophobicity and oleophobicity on the action of a substrate on contacting vesicles, providing a detailed explanation for the findings reported in ref 11 and a more general perspective on this issue.

2. METHODS

2.1. CG Description. The CG model proposed by the Martini force field is used here to describe the simulated molecules. This model is based on a 4-to-1 mapping, where on average four heavy atoms are represented by a single interactive bead, except for ringlike molecules that are mapped with a higher resolution [for instance, cholesterol (Chol) is described by a 3-to-1 resolution].[20] The model considers four main types of interactive beads: polar (P) and apolar (C) particles with a particular degree of polarity (from 1 = low polarity to 5 = high polarity) and nonpolar (N) and charged (Q) beads with specific hydrogen-bonding capabilities (d = donor, a = acceptor, da = both, and 0 = none). Ring particles are labeled by adding an "S". The Martini model has been successfully applied to study a large variety of lipid membrane phenomena.[21]

In our simulations, several molecular species are simulated. CG water particles are represented by highly polar "P4" bead particles, each one mapping four real water molecules. The phospholipid 1-palmitoyl-2-oleoylphosphatidylcholine (POPC) is formed by 13 interacting beads representing a positively charged choline group, a negatively charged phosphate, two neutral glycerols, and two tails with four and five apolar alkanelike particles (see Figure 1). The third bead of the longer acyl chain accounts for the unsaturation in the methylene sequence for the oleoyl tail. Chol is formed by eight particles: a polar bead for the hydroxyl group, five beads representing the ring sterol system, and two beads for the short alkyl tail (Figure 1).[20] The self-assembled alkanes forming the monolayer coatings are represented by a linear sequence of bonded apolar beads, each one representing four methylene groups (see subsection 2.3 and Figure 1). To mimic fluorinated groups, a new bead (F1) is added to the Martini list with the same apolar characteristics as the alkanelike particles, but 35% larger in interaction size according to reports from detailed atomistic simulations.[22]

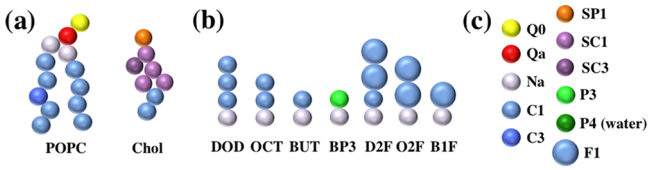

Figure 1. Schematic representation of the simulated molecules according to their CG Martini description. (a) POPC and Chol molecules forming the vesicle bilayer. (b) Self-assembled moieties forming the surface coating. (c) Martini codes for all particles used in the simulations.

2.2. Lipid Vesicle. A simulated vesicle system is built with 614 POPC and 263 Chol molecules (30 mol % of Chol). The inclusion of Chol provides the membrane vesicle with in-plane fluidity and flexibility properties similar to biological lipid membranes. The vesicle is hydrated with 71 552 water particles and conveniently equilibrated at a constant T = 310 K and p = 1 bar. The vesicle equilibrium size is of the order of 10 nm in diameter, 427 POPC molecules forming the outer leaflet and 187 POPC molecules forming the inner leaflet. Chol molecules flip-flop frequently between the two leaflets, the inner layer being more concentrated with Chol (35−40 mol %). Both leaflets display a fluid behavior, and no holes/pores are observed. The water density inside and outside of the vesicle becomes stabilized around 980 g/L.

2.3. Simulated Self-Assembled Monolayers. The coated surface consists of a 25 × 25 nm^2 surface of 4901 fixed and regularly placed silica-like particles (type "Na" in the Martini force field). The distance between the surface beads is smaller than their van der Waals size, so they overlap, leaving no gap in between. As suggested in other MD simulations[23] and to prevent water freezing, surface heterogeneity is accomplished by randomly replacing 10% of the silica-like particles with similar larger particles (radius of 0.55 nm instead of 0.47 nm) and a one-level reduction of attraction to all other particles.

Attached to the solid surface, we place different moieties, whose first particle bead is fixed to the solid substrate mimicking, for instance, the silane group commonly used to covalently link molecules to the SURFs. Different coating moieties are used in the simulations, varying the length of the attached compounds, their polar character, and their surface density in the monolayer. We simulate coatings of 20 × 20, 30 × 30, 40 × 40, and 50 × 50 molecules, which correspond to a lateral spacing of 1.25, 0.83, 0.625, and 0.5 nm, respectively. The lateral spacing value is in accordance with the experimental observations for alkyl-silane monolayers on silica.[24,25]

Different moieties are used to form the surface coating in the simulations, and they are all pictured in Figure 1 according to their CG description. We simulate monolayers of butane [$-(CH_2)_3-CH_3$, BUT], octane [$-(CH_2)_7-CH_3$, OCT], and dodecane [$-(CH_2)_{11}-CH_3$), DOD], which correspond to the molecules formed by 1, 2, and 3 CG particles, respectively, connected to the fixed silanelike bead. To mimic the effect of fluorinated silanes, we replace the last bead (B1F) or the last two beads (O2F and D2F) by a fluorinated "F1" particle that would represent a group of four fluorinated methylenes. For the sake of completeness, polar moieties (BP3) have also been simulated by linking polar beads (type "P3" in the Martini force field) to the fixed silane groups.

2.4. Simulation Protocols. The simulations are performed using the GROMACS v.4.5.5 software package.[26] The equilibrated vesicle is deposited on top of the coated surface at a distance of approximately 1.2 nm (see Figure 2). Periodic boundary conditions are applied along the x and y directions, and the temperature is fixed using a Berendsen

DOI: 10.1021/acs.langmuir.6b03364
Langmuir XXXX, XXX, XXX−XXX

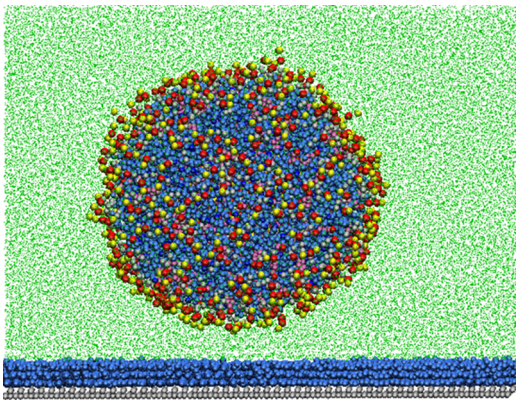

Figure 2. Initial surface/vesicle system configuration for the DOD_50 × 50 monolayer case. The color code is the same as in Figure 1. For clarity, water molecules are plotted as green dots.

coupling to 310 K. No pressure coupling is used, so the size of the x, y simulation plane remains constant. The surface particles and the first beads of the self-assembled moieties are fixed to their original positions during the simulation. In addition to what was commented earlier, 15% of antifreeze water[20] has also been used to prevent anomalous water freezing close to the vesicle and the monolayer surfaces. Electrostatic interactions are handled using a shifted Coulombic potential energy form, and the charges are screened with a relative dielectric constant ε_r = 15. Nonbonded interactions are cut off at 1.2 nm. The integration time step is set to 20 fs. The interpretation of the time scale in Martini simulations is not direct. The energy landscape is significantly "smoothed" due to the CG potentials with respect to atomistic approaches, so that the effective time scale is larger than the actual simulation time. Here, we used the standard conversion factor of 4,[20] which is the speed-up factor needed to capture the correct diffusional dynamics of CG water particles compared with real atomistic water molecules. Simulations of 4 μs are performed for each surface/vesicle system. In most of the simulations, the vesicle diffuses and contacts the coated surface during the first picoseconds. In a few cases, however, the vesicle diffuses away from the SAM and the simulation has to be restarted from a different initial configuration.

2.5. Wetting Properties. Water wettability of the simulated surfaces is analyzed by depositing a rectangular water box of 8 × 8 × 8 nm^3 made of 3800 water particles. The water box has been previously equilibrated at 310 K and an isotropic pressure of 1 bar. Once the water box is deposited on the monolayer, periodic boundary conditions are applied only along the x and y directions; the temperature is fixed to 310 K, and no pressure coupling is used. Short simulations of 160 ns are enough to observe how water wets the monolayer. Analogous simulations are performed to analyze oil wettability by using a rectangular box of 8 × 8 × 8 nm^3 made of 950 HD molecules formed by 4 C particles (3800 particles). Both water and oil wettabilities are quantified by estimating the CAs from the simulated equilibrium droplet profiles.[27]

3. RESULTS AND DISCUSSION

3.1. Three Modes of Action. The general effects of the simulated coated surfaces on the lipid vesicle can be classified according to three different modes of action involving distinctive consequences on vesicle configuration. First, moderately hydrophilic (polar) monolayers exhibit mode I where no vesicle adsorption is observed. The polar headgroups of the vesicle lipids attractively interact with the assembled molecules; however, because water particles also do so, the vesicle does not permanently attach to the SAM. The outer part of the vesicle eventually touches the monolayer, and it seems to roll on top of it. In any case, it preserves its integrity and the bilayer envelope configuration. At this point, it is important to notice that using more hydrophilic tips of the attached moieties, for instance, by the use of P4 and P5 Martini beads, does not result either in stable vesicle attachment or in the formation of supported lipid bilayers, as reported in previous molecular approaches for attractive surfaces.[17,18] In the Martini description, water molecules are at least as polar as the lipid headgroups, whereas the approaches in refs 17 and 18 use interaction parameters for the surface/lipid headgroup pairs that are artificially adjusted to extremely attractive values.[17,18] Martini-based simulations are not able to capture vesicle deposition unless oppositely charged lipids and substrates are used as reported in ref 19.

The second action mode is commonly found for densely packed fluorinated moieties, and it is illustrated in the molecular resolution in Figure 3 for the D2F_50 × 50 f3

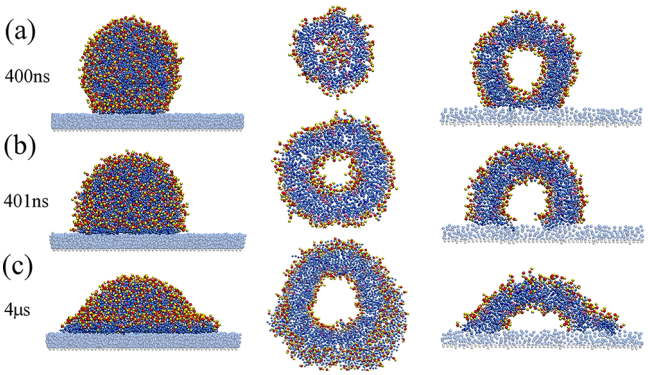

Figure 3. Action mode II illustrated by the D2F_50 × 50 monolayer case. The temporal sequence is plotted from top to bottom in the left column, and the corresponding cross sections in the monolayer plane just above the coated surface are seen in the middle column, and a central perpendicular plane is seen in the right column. The cross sections are 1 nm thick. The color code is the same as in Figure 1. Water and surface beads are not shown for clarity. The self-assembled moieties are plotted in "transparent" mode to distinguish from POPC tails. Different times are shown for (a) the initial contact, (b) the bilayer splitting, and (c) the stable thimblelike configuration.

monolayer case. In mode II, the vesicle initially contacts the monolayer, and because of the favorable interactions between the vesicle lipid tails and the hydrophobic surface, it spreads on the contacting base by breaking the outer leaflet at that point (Figure 3a). The inner leaflet is immediately broken, and a hole is opened in the contact region forming a rather circular and planar bilayer (central panel in Figure 3b). As a result, a thimblelike structure is formed where the bilayer configuration is preserved in the nonbroken part of the vesicle (left and right panels in Figure 3b). To increase the contact between the hydrophobic vesicle lipid tails and the self-assembled moieties, the resultant structure can be pushed down to some degree, slightly spreading the contacting circular bilayer and the vesicle hole on the base (Figure 3c). The volume constraint due to the solvent inside of the vesicle, however, does not allow further vesicle deformation, so the resultant thimblelike structure remains rather stable for the full simulation period. It is important to notice that no significant water leakage is detected during the adhesion process and the remaining duration of the simulations.

Finally, densely assembled alkane monolayers display action mode III, the most aggressive action mechanism. The attractive interaction between the hydrophobic molecular groups initially

DOI: 10.1021/acs.langmuir.6b03364
Langmuir XXXX, XXX, XXX−XXX

causes the formation of the thimblelike vesicle configuration as illustrated in Figure 3 for mode II. In these cases, however, the coated surface is able to rupture the vesicle, allowing the solvent to escape and spontaneously forming a continuous monolayer. This process consists of different stages that are presented in Figure 4a–e for the DOD_50 × 50 SAM and schematically

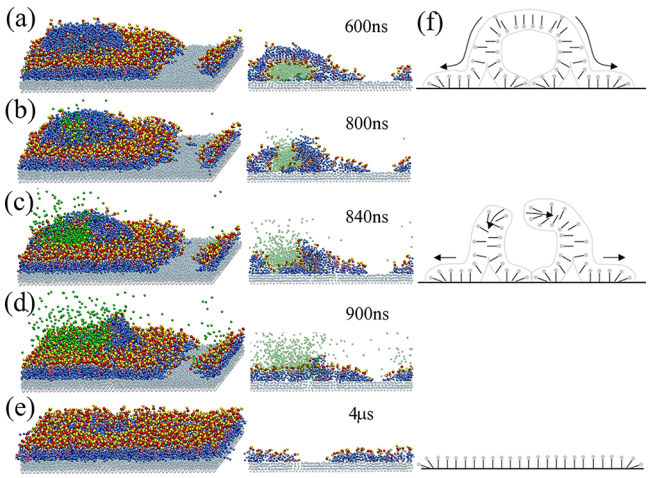

Figure 4. Action mode III illustrated by the DOD_50 × 50 monolayer case. The temporal sequence is plotted from top to bottom in the first column from the left, and the corresponding perpendicular cross section is seen in the central column. The cross sections are 1 nm thick. The color code is the same as in Figure 1. For clarity, only the water molecules initially contained inside of the vesicle are plotted and only for the first four exhibited times. The self-assembled moieties are plotted in "transparent" mode to distinguish from POPC tails. Different times are shown for (a) the spreading of the thimblelike configuration and (b–d) pore formation and development until (e) the final stable monolayer formation. (f) Schematic picture describing the different stages of the vesicle rupture (right column).

pictured in Figure 4f. Once the vesicle is adhered and the thimblelike structure is formed, the vesicle bilayer edge in contact with the SAM splits and separates, trying to form a monolayer (see Figure 4a and the top picture in Figure 4f). The inner leaflet spreads to a small extent toward the vesicle interior, whereas the outer layer is able to freely expand outward by extracting the lipids from the top of the vesicle and leaving some lipid tails exposed to water (notice the absence of lipid headgroups in the top of the vesicle in Figure 4a). Further spreading is then transiently arrested because of the volume constraint caused by the water molecules contained in the vesicle, and the resultant metastable configuration remains for a few tens of nanoseconds until a pore is formed (Figure 4b). As soon as this happens, the pore expands, the water escapes, and the remaining part of the vesicle rapidly retracts toward the substrate (Figure 4b–d). Simultaneously, the flat bottom spreads out until a stable lipid monolayer of vertically placed lipids is formed on top of the original coating SAM (Figure 4e). It is important to notice that the rupture of the absorbed vesicles displaying mode III is always due to the internal solvent pressure at a random position in the vesicle top where the polar "protection" in the outer leaflet has slid away to form the monolayer. This indicates a tension-driven pore formation mechanism as an alternative to the curvature-mediated rupture displayed during the supported bilayer formation in attractive substrates.[17,18]

So far, the simulations show that the different degrees of affinity between the assembled monolayer and the vesicle lipid tails determine the interaction mode to exhibit intact (mode I), partially absorbed (mode II), or ruptured and fully absorbed vesicles (mode III). Interestingly, one might have conjectured that increasing the hydrophobicity of the SAM coating would favor the contact between apolar lipid tails and assembled moieties, leading to more aggressive and destructive interactions. However, as observed by comparing Figures 3 and 4, the use of fluorinated monolayers exhibits less vesicle damage than alkane monolayers, although the former are more hydrophobic than the latter. This indicates that a deeper analysis of the energetics of vesicle adhesion has to be performed to assess the optimal conditions for vesicle collapse.

3.2. Energetics of Vesicle–SAM Interaction. The detailed analysis of the interaction energy for the three modes of action described above is done by plotting the temporal evolution of the van der Waals energy contributions attributed to the different pairs of contacts among the surface, SAM moieties, lipid molecules, and water particles (Figures 5–7). In this analysis, the energy contribution due to the

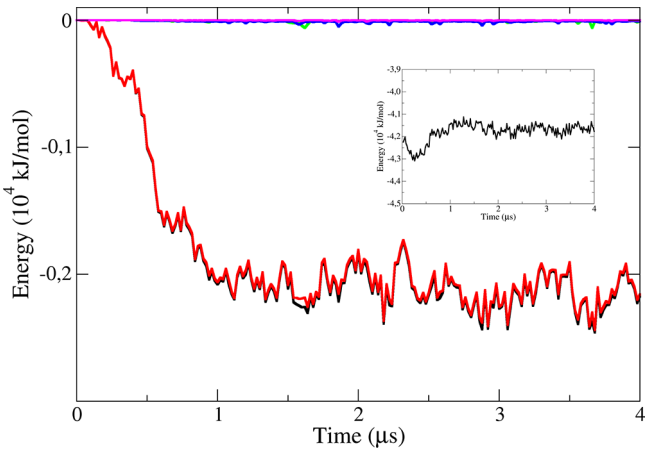

Figure 5. Temporal evolution of the van der Waals energy contribution because of the contact between the polar (BP3_50 × 50) SAM moieties and the vesicle. The energy of the interaction between the entire vesicle and the SAM (black line) is compared with the energies of the interaction between the SAM and the fragments of the vesicle lipid molecules (red: POPC_Head–SAM; green: POPC_Tail–SAM; blue: CHOL_Head–SAM; and magenta: CHOL_Tail–SAM). In the inset, the temporal evolution of the interaction energy between the SAM and water molecules is shown.

interaction between the entire vesicle and the substrate is compared with the contributions due to different fragments of the molecules forming the two subsystems: the POPC polar headgroup (POPC_Head), the POPC acyl tails (POPC_Tail), the Chol hydroxyl group (CHOL_Head), and the Chol apolar body (CHOL_Tail) for the vesicle, and the inner and final beads of the assembled moieties (SAM_in and SAM_top, respectively) and the SURF for the substrate. First, we analyze the three cases reported in the previous section that correspond to the densest SAMs (50 × 50). Notice that in these cases, the interactions of both the vesicle and the water molecules with the SURF are null and only the sum of SAM_in and SAM_top (SAM) contributions is shown. Between these two latter contributions, the largest one (more than 90%) corresponds to the ending beads (SAM_top), namely the P3, C1, or F1 beads. Therefore, the distinct interaction of these particles with the

DOI: 10.1021/acs.langmuir.6b03364
Langmuir XXXX, XXX, XXX–XXX

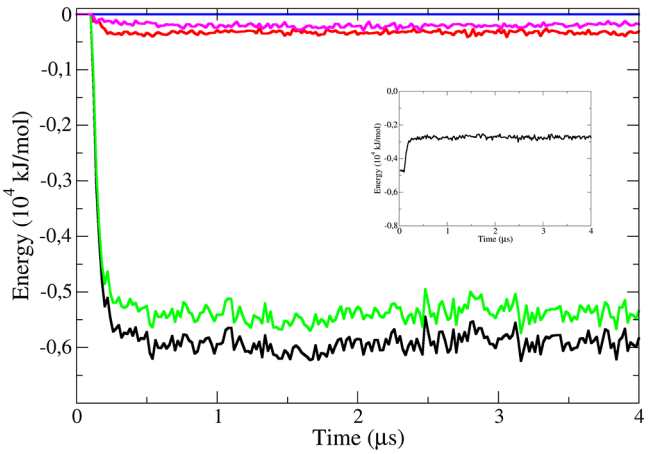

Figure 6. Temporal evolution of the van der Waals energy contribution because of the contact between the fluorinated (D2F_50 × 50) SAM moieties and the vesicle. The energy of the interaction between the entire vesicle and the SAM (black line) is compared with the energies of the interaction between the SAM and the fragments of the vesicle lipid molecules (red: POPC_Head−SAM; green: POPC_Tail−SAM; blue: CHOL_Head−SAM; and magenta: CHOL_Tail−SAM). In the inset, the temporal evolution of the interaction energy between the SAM and water molecules is shown.

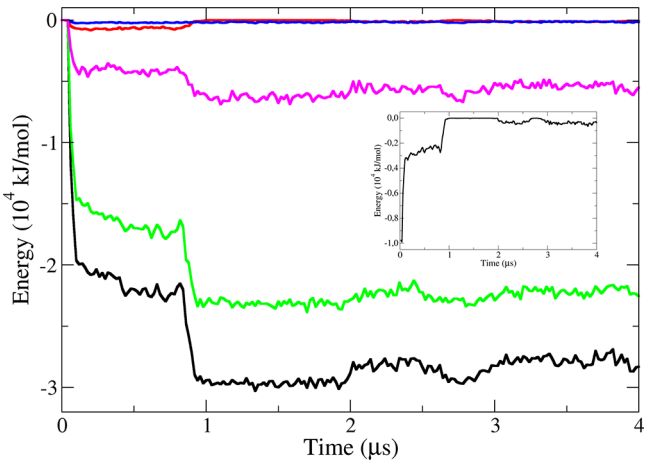

Figure 7. Temporal evolution of the van der Waals energy contribution because of the contact between the alkane (DOD_50 × 50) SAM moieties and the vesicle. The energy of the interaction between the entire vesicle and the SAM (black line) is compared with the energies of the interaction between the SAM and the fragments of the vesicle lipid molecules (red: POPC_Head−SAM; green: POPC_Tail−SAM; blue: CHOL_Head−SAM; and magenta: CHOL_Tail−SAM). In the inset, the temporal evolution of the interaction energy between the SAM and water molecules is shown.

water and lipid beads is what mostly determines the different interaction modes.

In general, the different modes of action are determined by the total energy gain (hereafter referred to adhesion energy) due to the replacement of water−SAM contacts by vesicle−SAM interactions. For polar coatings (mode I), the energy of the vesicle−SAM interaction displays a gain of about 2000 kJ/mol as soon as the vesicle contacts the SAM (Figure 5, black line). This gain is mainly due to the interaction between the polar tips of the assembled moieties and the POPC headgroups (Figure 5, red line), whereas the contribution due to Chol headgroups is much smaller because the Chol molecules are slightly inserted a little deeper inside of the inner region of the vesicle bilayer than POPC. As expected, the interaction with the hydrophobic vesicle lipid tails is minimal. Once the vesicle contacts the SAM, some water particles are put away from the coated surface, and this implies an energy cost of about 1500 kJ/mol (Figure 5, inset). The total energy balance yields an adhesion energy of about 500 kJ/mol, which is not sufficiently large to cause any vesicle deformation mode that would increase its interaction with the coated surface.

On the other hand, in the second action mode shown by the fluorinated D2F_50 × 50 case, the change in the contribution of SAM−water interaction energy is similar to the previous case (Figure 6, inset). By contrast, the energy gain due to the contact between the SAM and the vesicle (Figure 6, black line) more than compensates the energy loss due to the diminution of water−SAM contacts. Notice that the major contribution was from the interaction between the SAM and the POPC tails (Figure 6, green line) and, in a smaller degree, to Chol tails (Figure 6, violet line). The contacts between the lipid tails and the assembled moieties are produced during the formation of the thimblelike structure (Figure 3). The magnitude of the adhesion energy gain in this case (about 4000 kJ/mol) is enough to transform the vesicle into the thimblelike structure, but it is not sufficiently large to further deform this configuration and cause a complete vesicle rupture.

Finally, the energy profile for mode III, represented by the alkane DOD_50 × 50 case, evidences a two-step process (Figure 7, black line), as reported mechanistically in the previous section. A first energy gain occurs at the first contact of the vesicle with the SAM, and the formation of the thimblelike structure is observed as in mode II (Figures 4 and 6). Similarly, the main contributions to the energy gain are due to the interactions between the tail groups of the vesicle lipids (Figure 7, green and pink lines). This time, however, the magnitude of the adhesion energy (about 15 000 kJ/mol) is much larger than that in mode II. After a transient regime, a second decay is observed coinciding with the pore formation and expansion (Figure 4b−d), and the consequent formation of the lipid monolayer (Figure 4e). It is important to notice that although being less hydrophobic,[21] the vesicle lipid tail groups have a stronger affinity for the alkane moieties than for the fluorinated monolayer and, in consequence, more vesicle damage is observed. Moreover, water interaction energy (Figure 7, inset) first decreases at the thimblelike structure formation and, successively, it drops to small values when the lipid monolayer is formed. This indicates that the contact between water and the SAM is reduced to a minimum because a large part of the surface is covered by the POPC/Chol monolayer.

3.3. Effects of SAM Density and Length of Assembled Moieties. The effect of monolayer density and length of the assembled moieties in our simulations is illustrated in Figure 8, where the final 4 μs system configurations at different conditions are plotted. Whereas modes I and III are clearly identified by the conservation of vesicle configuration and the monolayer formation, respectively, mode II can be expressed in different degrees of vesicle deformation. For instance, the monolayers made of D2F moieties exhibit the action mode II at all simulated densities; however, the smaller the SAM density, the more regular and semispherical the thimblelike structure is, whereas for denser monolayers this structure is largely deformed and the salient small monolayer "tongues" can be

DOI: 10.1021/acs.langmuir.6b03364
Langmuir XXXX, XXX, XXX−XXX

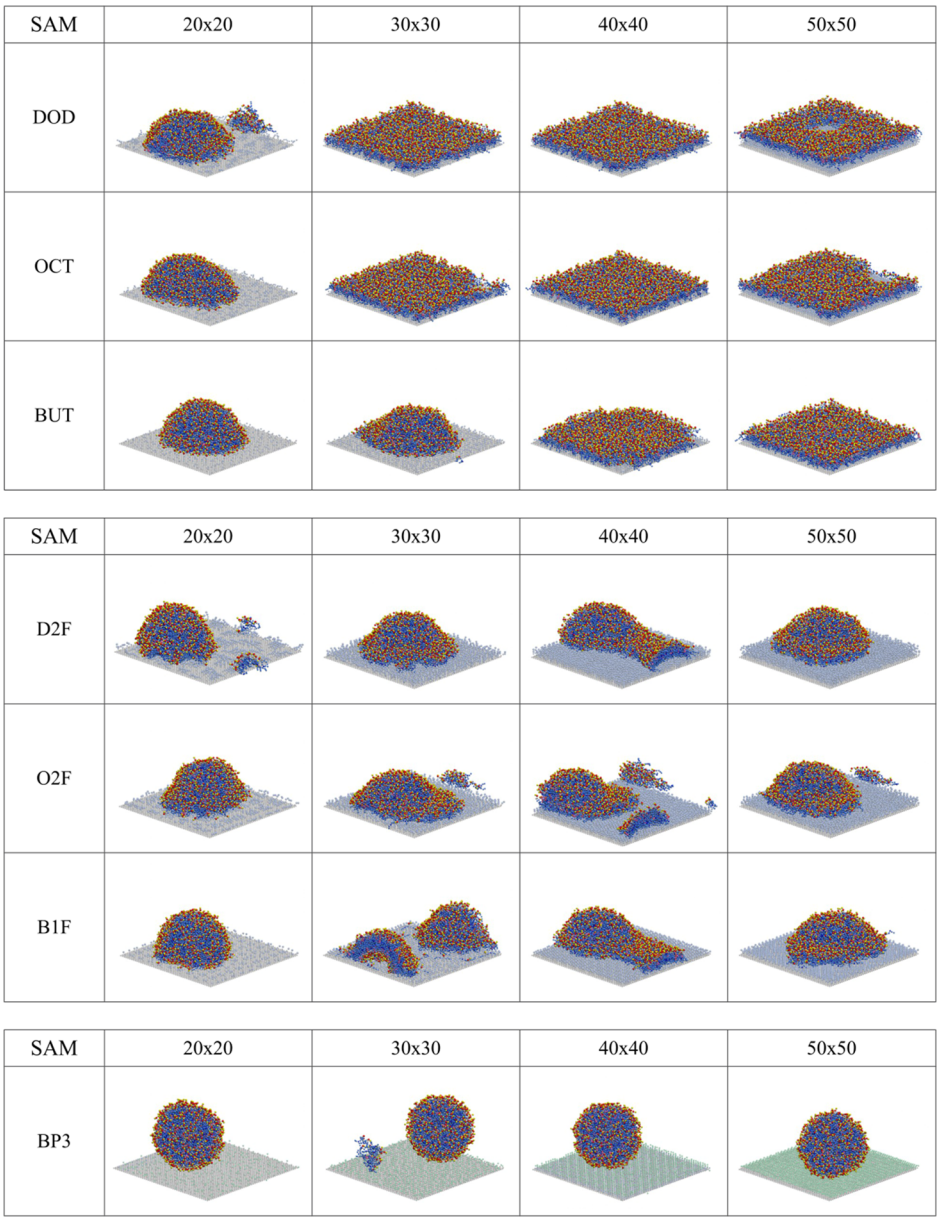

Figure 8. Final configuration of SAM−vesicle systems after the 4 μs simulation. From left to right: the configuration of the vesicle on SAMs made of molecules described in Figure 1b and with a density of 20 × 20, 30 × 30, 40 × 40, and 50 × 50 molecules in the 25 × 25 nm^2 surface. From top to bottom: the first three rows show the configuration of the vesicle on alkyl SAMs (DOD, OCT, and BUT); the next three rows show the configuration of the vesicle on fluorinated SAMs (D2F, O2F, and B1F); and the lowest row shows the configuration of the vesicle on polar SAM (BP3). The same color code as in Figures 1−4 is used.

observed. Accordingly, we could refer to a less or a more aggressive mode II.

To find the effect of SAM density, it is important to analyze separately the interaction energy contributions of the different fragments of the coated substrate (SURF, SAM_in, and SAM_top) with water and vesicle components. For the densest cases (50 × 50), the energy contributions from the substrate subsystem are practically determined by the interaction with the most external (SAM_top) group of beads; that is, the interaction with the SAM_in fragment is rather small (less than 10%), so is the interaction with the SURF particles (less than 1%). Instead, lower monolayer densities imply permeation of water and vesicle molecules to the inner beads of the assembled components and even reaching the SURF, and this modifies the energetics of the vesicle adhesion process.

A clear example is found for the DOD monolayer by comparing the 50 × 50 case leading to mode III (Figures 4 and 7) and the 20 × 20 case that results in mode II (Figure 9). Interestingly, in the latter case, even though the number of assembled molecules is much smaller, the energy gain due to the interaction between the vesicle components and the substrate is rather similar to that of the densest monolayer (20 500 kJ/mol and 22 000 kJ, respectively). This is due to the fact that vesicle lipid components penetrate the SAM, contacting not only the SAM_top fragment but also the inner beads of the assembled moieties and the silica substrate. Actually, these two latter contributions represent approximately 35 and 50%, respectively, of the total energy gain for the 20 × 20 monolayer (see Figure 9). On the other hand, water molecules are displaced from the substrate (most of them from

DOI: 10.1021/acs.langmuir.6b03364
Langmuir XXXX, XXX, XXX−XXX

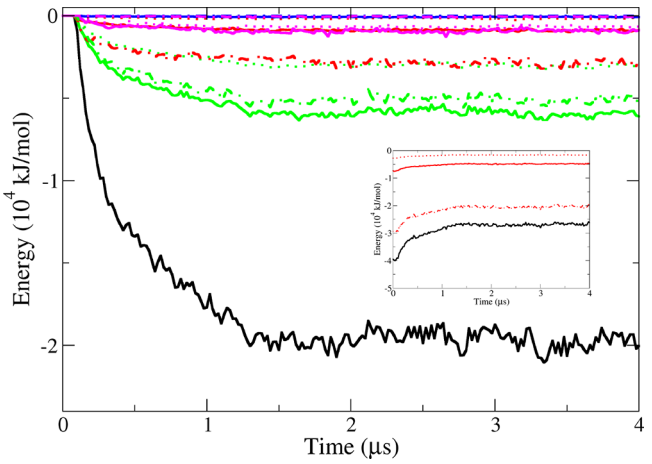

Figure 9. Temporal evolution of the van der Waals energy contribution due to the contact between the alkane (DOD_20 × 20) SAM moieties and the vesicle. The energy of the interaction between the entire vesicle and the substrate composed by the SAM and the SURF (black line) is compared with the energies of the interaction between the fragments of the vesicle lipid molecules and the substrate (red: POPC_Head−substrate; green: POPC_Tail−substrate; blue: CHOL_Head−substrate; and magenta: CHOL_Tail−substrate). The texture of the color lines corresponds to the interaction with the different substrate components: solid to SAM_in, dotted to SAM_top, and dot-dashed to SURF. In the inset, the temporal evolution of the interaction energy between the SAM and the water molecules is shown (black solid: water−substrate; red solid: water−SAM_in; red dotted: water−ASM_top; and red dot-dashed: water−SURF).

the SURF), yielding an energy cost (approximately 13 300 kJ/mol) larger than that for the 50 × 50 case (approximately 7000 kJ/mol). As a result, the total energy gain for the vesicle−SAM adhesion process for the 20 × 20 case (approximately 7200 kJ/mol) is approximately half the value found for the 50 × 50 coating, and therefore, mode II instead of mode III is obtained (Figure 8).

The length of the molecules forming the monolayer coating has also an effect on the adhesion process. As a general behavior, the shorter the coating moieties, the more accessible is the SURF to water and/or vesicle lipids. As a consequence, the hydrophobic character of the substrate is reduced and a less-aggressive adhesion mode is therefore observed. As expected, this effect is larger for lower SAM densities; compare, for example, the DOD_30 × 30 and BUT_30 × 30 cases in Figure 8.

3.4. Correlation between Wetting Properties and Action Modes. As reported so far, surface coatings with particular molecular characteristics (density, length, and polarity of assembled moieties) could be constructed to provide a desired mode of interaction with lipid vesicles. In principle, one may think of hydrophobicity to be the physicochemical property that comprehends the different molecular characteristics of the surface coating: hydrophobic substrates try to replace direct contact with water molecules by their association with hydrophobic acyl chains of vesicle lipids, thus breaking the vesicle bilayer configuration, whereas hydrophilic surfaces gain nothing with this exchange so that the interaction with a lipid vesicle is minimal. Monolayer hydrophobicity has been quantified in our MD simulations by the calculation of the CA for a water drop deposited on the analyzed substrate (see subsection 2.5 and the values provided in Table 1). Monolayers made of alkane moieties exhibit large water CAs, so that the interaction with a lipid vesicle results in its strong deformation and complete collapse (mode III). Within this group of SAMs, reducing the monolayer density and the components length causes substrate hydrophobicity to decrease, so that the resultant interaction mode III may be changed to the less destructive mode II (see Figure 8). On the contrary, polar coatings display small water CAs in coherence with the absence of vesicle deformation upon contact (mode I).

Table 1. Calculated CAs for Different Simulated Coated Substrates[a,b]

SAM	density	water CA (°)	hexadecane CA (°)
DOD	20 × 20	59	<10
	30 × 30	83	<10
	40 × 40	110	20
	50 × 50	111	10
DEC	20 × 20	40	10
	30 × 30	71	<10
	40 × 40	107	17
	50 × 50	106	<10
BUT	20 × 20	20	10
	30 × 30	53	<10
	40 × 40	95	15
	50 × 50	108	<10
D2F	20 × 20	82	NA
	30 × 30	122	89
	40 × 40	112	90
	50 × 50	125	86
O2F	20 × 20	103	60
	30 × 30	126	85
	40 × 40	115	89
	50 × 50	128	91
B1F	20 × 20	87	68
	30 × 30	117	94
	40 × 40	115	83
	50 × 50	124	90
BP3	20 × 20	<10	20
	30 × 30	<10	48
	40 × 40	<10	72
	50 × 50	<10	78

[a]Values of CA <10° mean that the CA is so small that it cannot be accurately measured. [b]Nonavailable (NA) entry corresponds to a droplet whose CA could not be calculated due to an irregular equilibrium shape.

The use of fluorocarbon coatings revealed, however, that hydrophobicity is not the unique factor that determines the SAM action mode. SAMs made of fluorinated components exhibit larger water CAs than alkane SAMs (Table 1) but display a less aggressive action mode upon contact with a lipid vesicle (Figure 8). As explained in the energetics analysis, fluorinated coatings do not favorably interact with water, but they do not do it with the hydrophobic lipid tails either. The extent of the latter effect is related to their oleophobicity that has been quantified in our MD simulation as the CA for a deposited oil (HD molecules according to the Martini model) drop on the analyzed substrate (see subsection 2.5 and the values provided in Table 1). Fluorinated coatings show not only a high hydrophobic character but also a significant oleophobic behavior so that they exhibit the intermediate action mode II on the interacting lipid vesicles. It is important

DOI: 10.1021/acs.langmuir.6b03364
Langmuir XXXX, XXX, XXX−XXX

at this point to comment on the origin of both the hydro- and oleophobicity of the fluorinated particles used in our CG approach. Following an atomistic approach,[22] it has been established that the larger hydrophobicity of fluorinated alkanes with respect to normal alkanes is due to their larger size that requires more work for cavity formation to accommodate a fluorocarbon compared with a hydrocarbon. The same effect would explain the oleophobicity exhibited here by fluorinated SAMs that, in turn, diminishes the strength of their interaction with the lipid vesicles.

The results reported so far establish a clear correlation between SAM wetting properties and adhesion action modes that is summarized in Figure 10. In this figure, water and oil

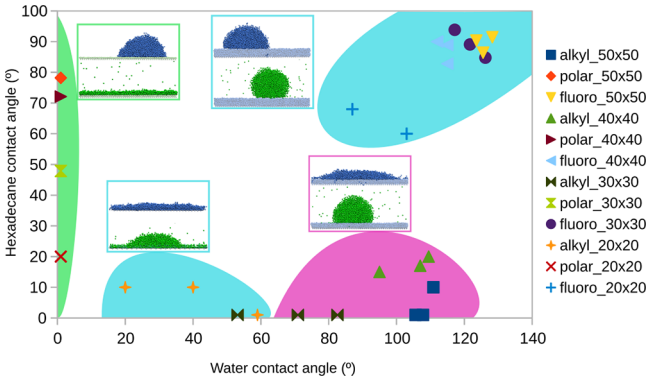

Figure 10. Behavior/morphological diagram as a function of the wetting characteristics of the coated surface. The inset panels show the configuration of water (green) and HD (blue) droplets deposited on the representative substrates for the four possible wetting regimes: hydrophilic/olephobic (top left), hydrophilic/olephilic (down left), hydrophobic/oleophilic (center), and hydrophobic/oleophobic (right). The symbols show the HD CAs plotted versus water CAs, and they are grouped according to the results shown in Figure 8 in regions corresponding to the three action modes, delimited by the green, light blue, and pink areas for modes I, II, and III respectively. The alkyl SAMs at density 20 × 20 and the BUT 30 × 30 (bottom left) are classified as hydrophilic/oleophilic and correspond to mode of action II (light blue area), whereas denser SAMs of longer alkanes (bottom right) are hydrophobic/olephilic and correspond to mode of action III (pink area). The fluorinated SAMs (top right) are classified as hydrophobic/oleophobic and correspond to mode of action II (light blue area). The polar SAMs (left) are highly hydrophilic with the olephobicity increasing with the density and show mode of action I (green area).

CAs are plotted for all simulated SAMs, providing a sort of behavior/morphological diagram that clearly shows distinct regions: a group of hydrophilic SAMs that exhibit action mode I, a region of hydrophobic and oleophobic coatings that result in mode II, and a region of hydrophobic and oleophilic SAMs that correspond to mode III. Moreover, a fourth group of hydrophilic and oleophilic SAMs that exhibit action mode II further confirms that both the hydrophobic and oleophilic characteristics of the SAM are accountable for the strong vesicle−SAM interaction that held to action mode III.

4. CONCLUSIONS

We have assessed different mechanisms of lipid vesicle interactions with surfaces coated by self-assembled monolayers of a variety of noncharged compounds and surface densities by using MD simulations. We have employed the Martini force field, a CG model that enables us to cover the length and time scales required to analyze this phenomenon, still retaining the molecular-level of the simulated system components. We are mostly interested in the effect of hydrophobic coatings that in some circumstances may cause the rupture of the bilayer structure of the vesicle. Given particular conditions on the polarity, length, and surface density of the self-assembled moieties covering the solid substrate, three distinctive modes of interactions have been recognized involving the absence of vesicle adhesion, partial adhesion together with vesicle deformation, and complete adhesion leading to vesicle destruction.

Our simulations clearly indicate that the vesicle adhesion onto solid surfaces can be adjusted by modifying their wetting properties. Polar (hydrophilic) coatings are not liable neither to adhere to nor even to deform the lipid vesicle upon contact. Instead, hydrophobic substrates made by attaching alkane moieties are able to strongly deform and break the vesicle configuration until forming a monolayer of vertically placed vesicle lipids. To do so, membrane rupture must take place at some point through tension-mediated pore formation and immediate expansion processes that have been analyzed at the molecular-level. Recently, it has been assessed that the interaction of lipid-enveloped entities, such as viruses, with solid−water interfaces is mainly governed by long-range electrostatics and the contributions due to the hydrophobic character of the solid substrate.[28] These contributions correspond to the energy gain from the reduction in the contact between water and apolar surfaces upon adhesion, and they are expected to increase by enhancing the hydrophobicity of the contacting substrate.[28] Interestingly, however, our simulations with fluorinated coatings indicate that increasing hydrophobicity does not necessarily optimize the adhesion effect if oleophobicity is also increased. In this case, replacing water molecules by apolar lipid tails at the contacting surface does not provide enough energy to burst the vesicle, and an intermediate action mode is found where the vesicle is partially adhered and deformed but still preserves part of its bilayer configuration. A complete analysis of the energetics involved at each action mode has been performed, confirming that higher adhesion energies are accomplished for hydrophobic/oleophilic substrates.

Our results are in direct agreement with the observations for the virus deactivation efficiency exhibited by a series of SURFs functionalized with neutral alkyl- and fluorosilanes.[11] Fluorinated compounds were proved to be less effective than alkane coatings, so that the strongest virus deactivation efficiency was accomplished for highly hydrophobic and oleophilic coated surfaces as supported by the outcome of our simulations. Comparison of our results with experimental observations, however, has to be cautious. Apart from the unavoidable limitations of the MD technique and the CG model used in our simulations, other aspects may alter the reported results. For example, the effect of surface roughness and/or the vesicle size, or the existence of preadsorbed lipid monolayer pieces may affect the different action modes. In addition, short microsecond-scale simulations are not able to capture the leakage of the vesicle content that occurs at the typical experimental time scales and that may lead to (slow) vesicle shrinking without requiring the rupture of the bilayer.

AUTHOR INFORMATION

Corresponding Authors

*E-mail: ilaria.mannelli@icfo.es (I.M.).

DOI: 10.1021/acs.langmuir.6b03364
Langmuir XXXX, XXX, XXX−XXX

*E-mail: reigada@ub.edu (R.R.).

ORCID

Ilaria Mannelli: 0000-0001-5322-839X

Notes

The authors declare no competing financial interest.

■ ACKNOWLEDGMENTS

The authors acknowledge the financial support from the Spanish Ministry of Economy and Competitiveness (MINECO) through project FIS 2013-41144P. The authors also acknowledge the financial support from the Spanish Ministry of Economy and Competitiveness (MINECO) through the "Severo Ochoa" Programme for Centres of Excellence in R&D (SEV-2015-0522), Fundació Privada Cellex, AGAUR 2014 SGR 1623, and Fondo Europeo de Desarrollo Regional (FEDER) through the grant TEC2013-46168-R. We are grateful to M. Lakadamyali for useful discussions.

■ REFERENCES

(1) Ratner, B. D.; Hoffman, A. S.; Schoen, F. J.; Lemons, J. E. *Biomaterials Science; An Introduction to Materials in Medicine*; Academic Press: London, 2004.

(2) Yebra, D. M.; Kiil, S.; Dam-Johansen, K. Antifouling technology—past, present and future steps toward efficient and environmentally friendly antifouling coatings. *Prog. Org. Coat.* **2004**, *50*, 75−104.

(3) Miura, Y.; Watanabe, Y.; Okabe, S. Membrane biofouling in pilot-scale membrane bioreactors (MBRs) treating municipal wastewater: Impact of biofilm formation. *Environ. Sci. Technol.* **2007**, *41*, 632−638.

(4) McConnell, H. M.; Watts, T. H.; Weis, R. M.; Brian, A. A. Supported planar membranes in studies of cell-cell recognition in the immune system. *Biochim. Biophys. Acta, Rev. Biomembr.* **1986**, *864*, 95−106.

(5) Tampé, R.; Dietrich, C.; Gritsch, S.; Elender, G.; Schmitt, L. In *Nanofabrication and Biosystems: Integrating Materials Science, Engineering and Biology*; Hoch, H. C., Jelinski, L. W., Craighead, H. G., Eds.; Cambridge University Press: New York, 1996.

(6) Bieri, C.; Ernst, O. P.; Heyse, S.; Hofmann, K. P.; Vogel, H. Micropatterned immobilization of a G protein-coupled receptor and direct detection of G protein activation. *Nat. Biotechnol.* **1999**, *17*, 1105−1108.

(7) Shahal, T.; Melzak, K. A.; Lowe, C. R.; Gizeli, E. Poly-(dimethylsiloxane)-Coated Sensor Devices for the Formation of Supported Lipid Bilayers and the Subsequent Study of Membrane Interactions. *Langmuir* **2008**, *24*, 11268−11275.

(8) Tu, Y.; Lv, M.; Xiu, P.; Huynh, T.; Zhang, M.; Castelli, M.; Liu, Z.; Huang, Q.; Fan, C.; Fang, H.; Zhou, R. Destructive extraction of phospholipids from *Escherichia coli* membranes by graphene nanosheets. *Nat. Nanotechnol.* **2013**, *8*, 594−601.

(9) Haldar, J.; An, D.; de Cienfuegos, L. Á.; Chen, J.; Klibanov, A. M. Polymeric coatings that inactivate both influenza virus and pathogenic bacteria. *Proc. Natl. Acad. Sci. U.S.A.* **2006**, *103*, 17667−17671.

(10) Hsu, B. B.; Wong, S. Y.; Hammond, P. T.; Chen, J.; Klibanov, A. M. Mechanism of inactivation of influenza viruses by immobilized hydrophobic polycations. *Proc. Natl. Acad. Sci. U.S.A.* **2011**, *108*, 61−66.

(11) Mannelli, I.; Reigada, R.; Suárez, I.; Janner, D.; Carrilero, A.; Mazumder, P.; Sagués, F.; Pruneri, V.; Lakadamyali, M. Functionalized surfaces with tailored wettability determine Influenza A infectivity. *ACS Appl. Mater. Interfaces* **2016**, *8*, 15058−15066.

(12) Xing, C.; Faller, R. Interactions of lipid bilayers with supports: A coarse-grained molecular simulation study. *J. Phys. Chem. B* **2008**, *112*, 7086−7094.

(13) Hoopes, M. I.; Deserno, M.; Longo, M. L.; Faller, R. Coarse-grained modeling of interactions of lipid bilayers with supports. *J. Chem. Phys.* **2008**, *129*, 175102.

(14) Hoopes, M. I.; Xing, C.; Faller, R. Multiscale modeling of supported lipid bilayers. In *Handbook in Modern Biophysics Vol. 2: Biomembrane Frontiers: Nanostructures, Models, and the Design of Life*; Jue, T., Faller, R., Longo, M. L., Risbud, S. H., Eds.; Springer, Humanta: Totowa, NJ, 2009; pp 101−120.

(15) Bennun, S. V.; Hoopes, M. I.; Xing, C.; Faller, R. Coarse-grained modeling of lipids. *Chem. Phys. Lipids* **2009**, *159*, 59−66.

(16) Hoopes, M. I.; Longo, M. L.; Faller, R. Computational modeling of curvature effects in supported lipid bilayers. *Curr. Nanosci.* **2011**, *7*, 716−720.

(17) Wu, H.-L.; Chen, P.-Y.; Chi, C.-L.; Tsao, H.-K.; Sheng, Y.-J. Vesicle deposition on hydrophilic solid surfaces. *Soft Matter* **2013**, *9*, 1908−1919.

(18) Fuhrmans, M.; Müller, M. Mechanisms of vesicle spreading on surfaces: Coarse-grained simulations. *Langmuir* **2013**, *29*, 4335−4349.

(19) Kong, X.; Lu, D.; Wu, J.; Liu, Z. Spreading of a unilamellar liposome on charged substrates: A coarse-grained molecular simulation. *Langmuir* **2016**, *32*, 3785−3793.

(20) Marrink, S. J.; Risselada, H. J.; Yefimov, S.; Tieleman, D. P.; de Vries, A. H. The MARTINI force field: Coarse grained model for biomolecular simulations. *J. Phys. Chem. B* **2007**, *111*, 7812−7824.

(21) Marrink, S. J.; Tieleman, D. P. Perspective on the Martini model. *Chem. Soc. Rev.* **2013**, *42*, 6801−6822.

(22) Dalvi, V. H.; Rossky, P. J. Molecular origins of fluorocarbon hydrophobicity. *Proc. Natl. Acad. Sci. U.S.A.* **2010**, *107*, 13603−13607.

(23) de Moura, A. F.; Bernardino, K.; Dalmaschio, C. J.; Leite, E. R.; Kotov, N. A. Thermodynamic Insights into the Self-Assembly of Capped Nanoparticles Using Molecular Dynamic Simulations. *Phys. Chem. Chem. Phys.* **2015**, *17*, 3820−3831.

(24) Graupe, M.; Takenaga, M.; Koini, T.; Colorado, R., Jr.; Lee, T. R. Oriented Surface Dipoles Strongly Influence Interfacial Wettabilities. *J. Am. Chem. Soc.* **1999**, *121*, 3222−3223.

(25) Sellers, H.; Ulman, A.; Shnidman, Y.; Eilers, J. E. Structure and Binding of Alkanethiolates on Gold and Silver Surfaces: Implications for Self-Assembled Monolayers. *J. Am. Chem. Soc.* **1993**, *115*, 9389−9401.

(26) Lindahl, E.; Hess, B.; van der Spoel, D. Gromacs 3.0: A package for molecular simulation and trajectory analysis. *J. Mol. Model.* **2001**, *7*, 306−317.

(27) Sergi, D.; Scocchi, G.; Ortona, A. Molecular Dynamics Simulations of the Contact Angle between Water Droplets and Graphite Surfaces. *Fluid Phase Equilib.* **2012**, *332*, 173−177.

(28) Armanious, A.; Aeppli, M.; Jacak, R.; Refardt, D.; Sigstam, T.; Kohn, T.; Sander, M. Viruses at Solid−Water Interfaces: A Systematic Assessment of Interactions Driving Adsorption. *Environ. Sci. Technol.* **2016**, *50*, 732−743.

DOI: 10.1021/acs.langmuir.6b03364
Langmuir XXXX, XXX, XXX−XXX